Femtosecond dynamics of the forbidden carotenoid S_1 state in light-harvesting complexes of purple bacteria observed after two-photon excitation

Peter J. Walla, Patricia A. Linden, Chao-Ping Hsu, Gregory D. Scholes, and Graham R. Fleming*

Department of Chemistry, University of California, and Physical Biosciences Division, Lawrence Berkeley National Laboratory, Berkeley, CA 94720-1460

Edited by Robin M. Hochstrasser, University of Pennsylvania, Philadelphia, PA, and approved July 19, 2000 (received for review May 19, 2000)

Time-resolved excited-state absorption intensities after direct two-photon excitation of the carotenoid S_1 state are reported for light-harvesting complexes of purple bacteria. Direct excitation of the carotenoid S_1 state enables the measurement of subsequent dynamics on a fs time scale without interference from higher excited states, such as the optically allowed S_2 state or the recently discovered dark state situated between S_1 and S_2. The lifetimes of the carotenoid S_1 states in the B800-B850 complex and B800-B820 complex of *Rhodopseudomonas acidophila* are 7 ± 0.5 ps and 6 ± 0.5 ps, respectively, and in the light-harvesting complex 2 of *Rhodobacter sphaeroides* ≈1.9 ± 0.5 ps. These results explain the differences in the carotenoid to bacteriochlorophyll energy transfer efficiency after S_2 excitation. In *Rps. acidophila* the carotenoid S_1 to bacteriochlorophyll energy transfer is found to be quite inefficient (ϕ_{ET1} <28%) whereas in *Rb. sphaeroides* this energy transfer is very efficient (ϕ_{ET1} ≈80%). The results are rationalized by calculations of the ensemble averaged time constants. We find that the Car $S_1 \rightarrow$ B800 electronic energy transfer (EET) pathway (≈85%) dominates over Car $S_1 \rightarrow$ B850 EET (≈15%) in *Rb. sphaeroides*, whereas in *Rps. acidophila* the Car $S_1 \rightarrow$ B850 EET (≈60%) is more efficient than the Car $S_1 \rightarrow$ B800 EET (≈40%). The individual electronic couplings for the Car $S_1 \rightarrow$ BChl energy transfer are estimated to be approximately 5–26 cm^{-1}. A major contribution to the difference between the energy transfer efficiencies can be explained by different Car S_1 energy gaps in the two species.

Plants and some bacteria have achieved remarkably high efficiencies of solar light conversion in photosynthesis. Recently, high-resolution crystal structures of some peripheral light-harvesting complexes of photosynthetic purple bacteria (1–3) have become available, enabling us to study the basic principles of the highly efficient collection of solar energy (4–8). In the light-harvesting complexes of purple bacteria, such as light-harvesting complex 2 (LH2) of *Rhodobacter sphaeroides* or *Rhodopseudomonas acidophila*, carotenoids (Cars) play important roles as light-harvesting and photoprotective pigments, as they do in the chloroplasts of higher plants (9, 10). In *Rb. sphaeroides* >95% of the photons absorbed by the Cars are transferred as excitation energy to the reaction center; in the strain 7050 of *Rps. acidophila,* which is the strain used in this report, the corresponding number is ≈70% (9, 11, 12). In the subunits of the B800-B850 complex of *Rps. acidophila* there is one Car (rhodopin glucoside) molecule per two bacteriochlorophyll (BChl) molecules in the B850 ring and one BChl in the B800 ring (1). Nine of these subunits comprise the LH2 ring, B800-B850 complex, of *Rps. acidophila*. Spectroscopic and biochemical reports suggest that the structures of the B800-B820 complex of *Rps. acidophila* and LH2 of *Rb. sphaeroides* (with the Car spheroidene) are similar (13, 14).

Despite intensive investigation of the underlying mechanisms (8, 10, 12, 15–20), many aspects of the electronic energy transfer (EET) from the Cars are still poorly understood. The electronic states of Cars often are described by analogy to polyenes (Fig. 1): Their ground state (S_0) and first excited state (S_1) both possess A_g^- symmetry, their second excited state (S_2) possesses B_u^+ symmetry in the idealized C_{2h} point group. Only the $S_0 \leftrightarrow S_2$ transition is optically dipole-allowed. Excitation of S_2 is followed by very rapid (τ_{21} ≈100–200 fs) internal conversion (IC) to S_1, which means that a significant fraction of the excitation energy flows through this state (21). However, because the $S_1 \rightarrow S_0$ transition is dipole-forbidden it remains a challenge to elucidate the mechanism that promotes Car S_1 to Chl EET. Neither the Förster (22, 23) nor Dexter theories (24) provide satisfactory predictions (15, 20). To explore this issue, several authors have deconvoluted Car $S_1 \rightarrow$ BChl EET time constants, τ_{ET1}, from pump-probe or up-conversion data obtained after excitation of the Car S_2 state in different species. A few examples of time constants derived in this way are: peridinin to chlorophyll *a* (Chl *a*) EET in the peridinin-Chl *a*-protein (PCP) from *Amphidinium carterae* (PCP; 3.1 ps), spheroidene to BChl EET in *Rb. sphaeroides* (2.0 ps) and okenone to BChl *a* ET in *Chromaticum purpuratum* (3.8 ps and 0.5 ps) (19, 25, 26). However, the best way to find direct evidence for Car $S_1 \rightarrow$ BChl EET and to determine its contribution to the overall Car $\rightarrow$ BChl EET is to excite Car S_1 exclusively and thereby measure τ_{ET1} and ϕ_{ET1} directly without any convolution with S_2 state dynamics. This approach becomes even more important considering the recent identification of another dark state in spheroidene at ≈17,600 cm^{-1} between the S_1 and the S_2 states of Cars (18). This state has B_u^- symmetry and is thought to play an important role in facilitating the Car $S_2 \rightarrow$ Car S_1 IC (27). However, a transition $A_g^- \leftrightarrow B_u^-$ is neither one-photon allowed nor two-photon allowed and therefore does not contribute to our two-photon results.

An elegant way to populate S_1 directly is by two-photon excitation (TPE) because transitions between states of A_g symmetry are two-photon allowed. Recently we have found evidence for Car $S_1 \rightarrow$ BChl EET in *Rb. sphaeroides* by measuring the Car TPE spectrum through the steady-state BChl fluorescence (see Fig. 1) (28). We obtained similar results in the light harvesting complex LHCII of higher plants and green algae (29).

In this work we report fs time-resolved excited-state absorption (ESA) of the Car S_1 state in three light-harvesting complexes of purple bacteria observed after TPE of this state. We report resuts for the B800-B850 and B800-B820 LH2s of *Rps. acidophila* and the LH2 of *Rb. sphaeroides*. To understand the mechanism that promotes this EET, we model the dynamics by using a theory that calculates the ensemble average energy transfer rates using as inputs the site energy disorder and the

This paper was submitted directly (Track II) to the PNAS office.

Abbreviations: EET, electronic energy transfer; Car, carotenoid; BChl, bacteriochlorophyll; Chl, chlorophyll; ESA, excited-state absorption; TPE, two-photon excitation; LH2, light-harvesting complex 2 of purple bacteria; IC, internal conversion; DOS, density of states.

*To whom reprint requests should be addressed. E-mail: GRFleming@lbl.gov.

The publication costs of this article were defrayed in part by page charge payment. This article must therefore be hereby marked "*advertisement*" in accordance with 18 U.S.C. §1734 solely to indicate this fact.

Article published online before print: *Proc. Natl. Acad. Sci. USA*, 10.1073/pnas.190230097. Article and publication date are at www.pnas.org/cgi/doi/10.1073/pnas.190230097

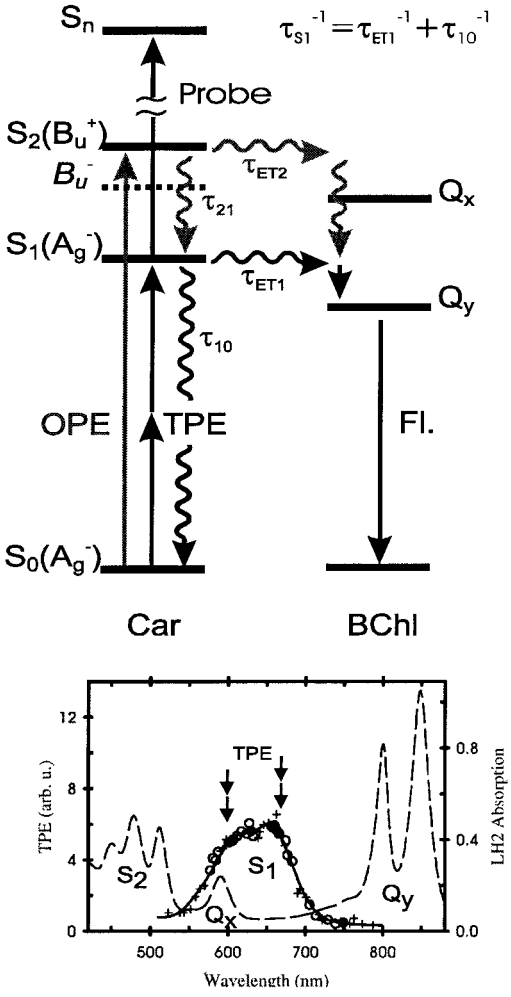

Fig. 1. (*Upper*) Energy diagram for LH2. Black arrows indicate energy pathways occurring in the TPE pump probe experiment. Gray arrows indicate additional energy pathways in conventional one-photon experiments. OPE, One-photon excitation. Fl., Fluorescence. τ_{ET2}, Time constant for Car $S_2 \rightarrow$ BChl EET [≈50 fs (30)]. τ_{21}, Time constant for Car $S_2 \rightarrow S_1$ IC [≈135 fs (30)]. τ_{ET1}, Time constant for Car $S_1 \rightarrow$ BChl EET. τ_{10}, Time constant for Car $S_1 \rightarrow S_0$ IC. τ_{S1}, $(\tau_{ET1}^{-1} + \tau_{10}^{-1})^{-1}$ lifetime of the Car S_1 state measured in this work. (*Lower*) TPE spectrum of LH2 of *Rb. sphaeroides* (line with symbols), one-photon absorption spectrum (dashed line). Data taken from ref. 28. TPE-wavelengths for the TPE pump probe experiment are indicated with double arrows.

electron–phonon coupling of the chromophores as well as the excitonic nature of the acceptors.

Experimental Procedures

LH2 of *Rb. sphaeroides* was prepared from the *Rb. sphaeroides* strain 2.4.1 by using previously described methods (28). LH2s of *Rps. acidophila* were isolated from *Rps. acidophila* strain 7050 by using the methods described in refs. 9 and 30. β-Carotene (Acros, New Jersey) was dissolved in octane by sonicating for ≈10 s and centrifuging for 4 min at ≈8,000 g. The solutions had an optical density of ≈1 per mm at the maximum of the absorption. The samples were flowed through a 1-mm pathlength quartz cell and maintained at 4°C under a nitrogen atmosphere. To reduce scattering further, a 0.45 μm filter was added to the flow cycle. The pump-pulses [≈10 nJ, 85 fs full width half maximum (FWHM), 250 kHz] and white-light probe pulses were both provided by a Coherent 9450 optical parametric amplifier. Excitation light intensity fluctuations were monitored with a power meter connected to a computer. To minimize population via one-photon excitation caused by the probe-white light we blocked the dominant 800-nm component with a highly reflective laser mirror and filtered the probe wavelength with a 555 ± 5-nm interference filter before the sample cell. The pump beam was focused with an f = 5-cm achromatic lens and the probe beam with an f = 10 cm. Only about <25% of the intensity of both beams was blocked by a 50-μm pinhole. Our instrument response function had a FWHM of ≈90 fs. The signal was detected by using a photodiode and lock-in amplification. To suppress white-light fluctuations with a frequency similar to the pump-chopper frequency, a part of the white light was measured with a separate photodiode and lock-in amplifier also triggered by the chopper. Subtracting this trace resulted in an improvement of the signal-to-noise ratio of more than a factor of 5. The polarization dependence was measured by using a 1,310-nm λ/4 and λ/2-waveplate in the excitation beam. Results without a waveplate were identical to those with λ/2-waveplate.

Results

β-Carotene in octane solution, a Car with known properties and similarities with spheroidene (31), was used to test the experimental setup. From one-photon pump probe data it is known that ESA from the S_1 of Cars has a maximum close to 550 nm, therefore we chose this wavelength as the detection wavelength in all experiments (32). The excitation wavelength was ≈1,310 nm, which is close to the 0–0 transition of the S_1 two-photon absorption of the Car (Fig. 1.). The changes in the probe intensity after TPE were typically on the order of 0.1%. A monoexponential fit to the transient absorption data gave a time constant of 9 ± 0.2 ps, in excellent agreement with the reported S_1 lifetime of β-carotene (31).

Two experiments were used to confirm that the pump was a two-photon process. First, the power dependence of the signal intensities were found to have a quadratic dependence on the excitation power (Fig. 2*b*). The fit suggests a power dependence with an exponent of 2.2 ± 0.3. Second, we measured the dependence of the signal on the polarization of the two-photon pump pulse (33). In one-photon spectroscopy the signal depends only on the relative orientation of linear polarized pump and probe fields. In two-photon spectroscopy, the signal is in general different for linear, circular, or any elliptical polarization of the pump beam. The polarization ratio, $\Omega = S_{circ}/S_{lin}$, defined as the ratio of the signal obtained with circularly and with linearly polarized excitation, depends on the symmetries of the excited- and ground-state wave functions. Therefore this experiment can be used not only to verify the two-photon nature of the signals, but also to identify the symmetry of the two-photon excited molecule via its polarization ratio Ω. This can be used to confirm that we have indeed excited the Car in the light-harvesting complexes. The result, shown in Fig. 2*c*, gives Ω = 0.84 ± 0.07, which is identical within error to the literature value of Ω ≈ 0.8 for all-trans diphenyloctatetraene and diphenylhexatriene (34).

In Fig. 3*a* the time dependence of the ESA is shown for the LH2 of *Rb. sphaeroides* and the B800-B850 and B800-B820 LH2 of *Rps. acidophila* observed after TPE at 1,310 nm. All traces show a decay on the ps time scale to a constant offset, which persists over the entire dynamic range accessible with our setup (≈400 ps). The results of fits to $OD(t) = y_0 + Ae^{-t/\tau_{S1}}$ are summarized in Table 1. A relatively fast decay with a time constant of $\tau_{S1} \approx 1.9 \pm 0.5$ ps is observed for *Rb. sphaeroides*, whereas both complexes of *Rps. acidophila* show a significantly slower decay ($\tau_{S1} \approx 7 \pm 0.5$ ps and $\tau_{S1} \approx 6 \pm 0.5$ ps). The observed τ_{S1} for *Rb. sphaeroides* is in very good agreement with the value recently reported by Koyama and coworkers (19). As Fig. 3*b* shows, the preexponential factor A has a quadratic dependence on the excitation power, the solid line in Fig. 3*b* being fit by an exponent of 2.2 ± 0.3. We assign the decay

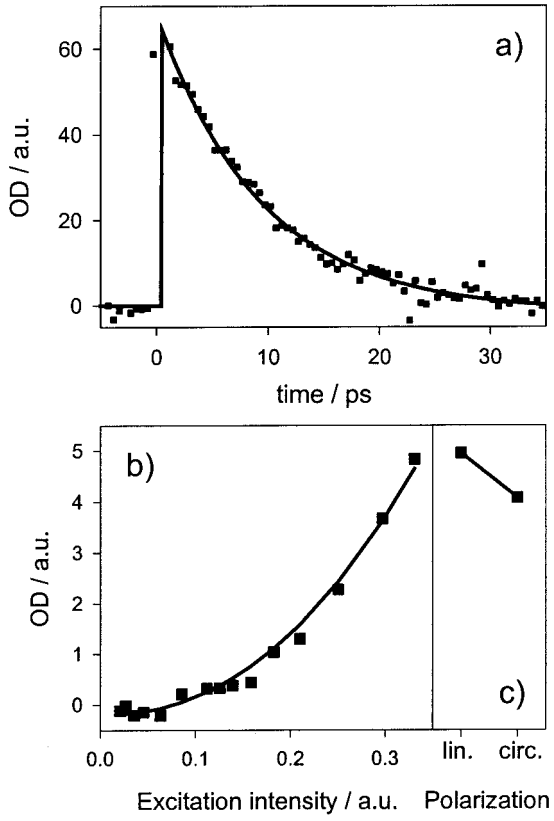

Fig. 2. (*a*) Time dependence of ESA (λ_{det} = 550 nm) of β-carotene in octane (squares) observed after TPE (λ_{exc} = 1,310 nm). Monoexponential fit: 9 ± 0.2 ps (solid line). (*b*) Power dependence of ESA. Power fit: Exponent = 2.2 ± 0.3 (solid line). (*c*) Relative intensity of ESA excited with linear and circular polarized light (Ω = 0.84 ± 0.07). The ''coherence spike'' is very large in the two-photon experiments (off scale) and has a quadratic dependence on the excitation power and a linear dependence on the Car concentration. No spike was seen with a pure buffer sample. In experiments with chlorophyll *a*, which has no two-photon allowed states, the coherence spike was found to be substantially smaller in magnitude (data not shown).

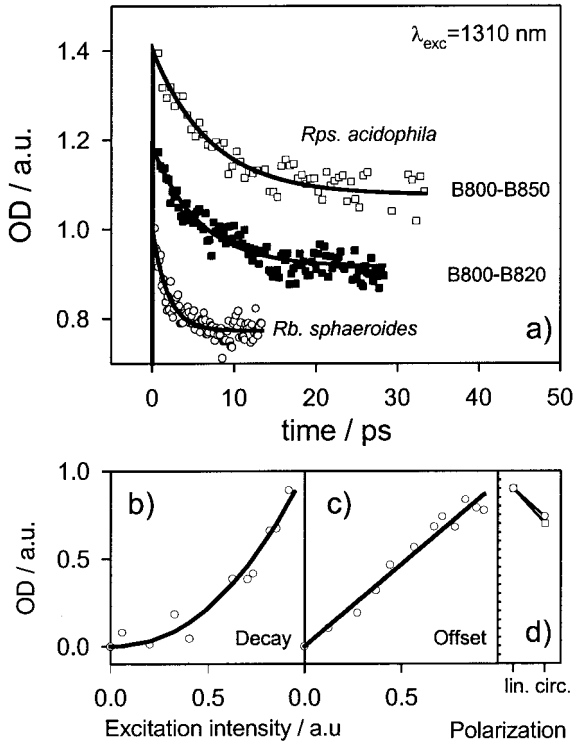

Fig. 3. (*a*) Time dependence of ESA (λ_{det} = 550 nm) along with monoexponential fits with constant offset of the B800-B850 complex (□, τ_{S1} = 7 ± 0.5 ps) and the B800-B820 complex (■, τ_{S1} = 6 ± 0.5 ps) of *Rps. acidophila* and LH2 of *Rb. sphaeroides* (○, τ_{S1} = 1.9 ± 0.5 ps) observed after TPE (λ_{exc} = 1,310 nm). The traces have been normalized and offset from each other by 0.2. (*b*) Power dependence of the prefactor in the monoexponential fit to the data of *Rb. sphaeroides* (○). Power fit: Exponent = 2.2 ± 0.3 (solid line). (*c*) Power dependence of the constant offset in the fit to the data of *Rb. sphaeroides* (○). Solid line: Linear fit. (*d*) Relative intensity of the fluorescence obtained after TPE (λ_{exc} = 1,310 nm) with linear and circular polarized light of B800-B850 of *Rps. acidophila* (□, Ω = 0.80 ± 0.04) and LH2 of *Rb. sphaeroides* (○, Ω = 0.84 ± 0.04).

component as the lifetime, τ_{S1}, of the S_1 state of the Cars in the light-harvesting complexes. Further confirmation of this assignment is provided by the polarization dependence shown in Fig. 3*c*. In both species the observed polarization ratio is very similar to those observed for β-carotene and polyenes (34) in solution (Ω = 0.84 ± 0.04 for *Rb. sphaeroides* and Ω = 0.80 ± 0.04 for *Rps. acidophila*).

The constant offset y_0 has a linear dependence on the excitation power (Fig. 3*c*). No constant offset can be seen with pure buffer as sample. This result can be explained as a direct excitation of triplet states. It is not surprising that, with the given field intensities, the probability of directly exciting a spin forbidden transition via one-photon excitation is similar to the probability of exciting the S_1 state via TPE. However, because no offset has been observed with Cars in solution, we must assume that it is the triplet state of the BChl that can be seen in the transient absorption of the light-harvesting complexes. This interpretation is supported by the fact that the ESA of the triplet states of BChl has a maximum close to the detection wavelength of 550 nm and that the triplet states are the only states with an energy corresponding to one-photon excitation at 1,310 nm (35). For the interpretation of the S_1 state dynamics the triplet state excitation can be neglected, because the overall population of excited states is very small.

In Fig. 4 the time-resolved data of the Car S_1 ESA for all species are shown analogously to Fig. 3*a* but with TPE at 1,200 nm. As can been seen from Fig. 1, an excitation wavelength of 1,200 nm corresponds to the blue edge of the TPE spectrum of the light-harvesting complexes. The kinetics are very similar to the kinetics observed after TPE at 1,310 nm. We observe a relatively fast decay with the time constant $\tau_{S1} \approx 3 \pm 0.5$ ps for *Rb. sphaeroides*, whereas both complexes of *Rps. acidophila* show a significantly slower decay: $\tau_{S1} \approx 7 \pm 0.5$ ps and $\tau_{S1} \approx 7.5 \pm 0.5$ ps. However, the data, especially from *Rb. sphaeroides*, are not fit as well by a monoexponential decay as the data for TPE at 1,310 nm. This is possibly related to the 2,000 cm^{-1} of excess vibrational energy resulting from 1,200-nm excitation compared with 1,310 nm. Another difference between the data observed with TPE at 1,200 nm and that at 1,310 nm is the significantly smaller relative magnitude of the constant offset (see Table 1). We will use the time constants observed with excitation at 1,310 nm for our subsequent analysis.

Discussion

Efficiencies of the Energy Transfer Via the Car S_2 and the Car S_1 States. The significantly quenched Car S_1 lifetime observed after direct TPE of *Rb. sphaeroides*, $\tau_{S1} \approx 1.9 \pm 0.5$ ps, compared with the lifetime of spheroidene in solution, $\tau_{10} \approx 9$ ps (31), provides clear evidence for efficient Car $S_1 \rightarrow$ BChl EET. We calculate τ_{ET1} for *Rb. sphaeroides*, assuming τ_{10} is unchanged, to be $\tau_{ET1} = (\tau_{S1}{}^{-1}$

Table 1. Fitting results for the kinetic data in Figs. 2–4 and the corresponding polarization ratios

λ_{exc}/nm	1310				1200		
Species	β-carotene	*Rb. sphaeroides*	*Rps. acidophila* B800–B850	*Rps. acidophila* B800–B820	*Rb. sphaeroides*	*Rps. acidophila* B800–B850	*Rps. acidophila* B800–B820
τ_{S1}/ps	9 ± 0.5	1.9 ± 0.5	7 ± 0.5	6 ± 0.5	3 ± 0.5	7 ± 0.5	7.5 ± 0.5
A/%	100	41	38	34	46	45	46
y_0/%	0	59	62	66	54	55	54
Ω	0.84 ± 0.07	0.84 ± 0.04	0.80 ± 0.04	—	—	—	—

$OD(t) = y_0 + Ae^{-t/\tau_{S1}}$; $\Omega = S_{circ}/S_{lin}$.

$- \tau_{10}^{-1})^{-1} \approx 2.4 \pm 0.5$ ps. The unquenched S_1 lifetime of the Car in *Rps. acidophila*, rhodopin glucoside, has been determined by Frank and coworkers (36) to be $\tau_{10} \approx 4.1$ ps. We measured $\tau_{S1} \approx 6$–7 ps in the antenna complex, indicating that Car $S_1 \rightarrow$ BChl EET is negligible in *Rps. acidophila*. Even if the time constant for IC of rhodopin glucoside in the protein is as long as $\tau_{10} \approx 9$ ps, like the corresponding value for β-carotene or spheroidene in solution, the Car $S_1 \rightarrow$ BChl EET time τ_{ET1} could not be faster than 25 ps, and the Car $S_1 \rightarrow$ BChl EET efficiency ϕ_{ET1} then would be $\phi_{ET1} = (\tau_{S1}^{-1} - \tau_{10}^{-1})\ \tau_{S1} < 28\%$.† The same calculation for *Rb. sphaeroides*, using the value $\tau_{10} = 9$ ps for spheroidene, yields a Car $S_1 \rightarrow$ BChl EET efficiency of $\phi_{ET1} \approx 80\%$.

Using the known values for the overall Car $\rightarrow$ BChl EET quantum yield, ϕ_{OA}, together with the values of ϕ_{ET1} we are able to calculate the energy transfer efficiencies for Car $S_2 \rightarrow$ BChl EET, ϕ_{ET2}. The overall EET efficiency is the sum of both efficiencies, weighted by their population probabilities: $\phi_{OA} = \phi_{ET2} + \phi_{ET1}\phi_{21}$, where ϕ_{21} is the quantum efficiency for Car $S_2 \rightarrow$ Car S_1 IC, $\phi_{21} = \tau_{21}^{-1}/(\tau_{ET2}^{-1} + \tau_{21}^{-1}) = 1 - \phi_{ET2}$ (see Fig. 1). We now assume that ϕ_{OA} differs from 100% entirely owing to Car $S_1 \rightarrow$ Car S_0 IC. The quantum yield for Car $S_1 \rightarrow$ Car S_0 IC is $\phi_{10} = (1 - \phi_{ET1})\phi_{21}$. Therefore ϕ_{OA} also can be written as $\phi_{OA} = 1 - [(1 - \phi_{ET1}) \times \phi_{21}] = 1 + (\phi_{ET1} - 1) \times \phi_{21}$. Substituting $\phi_{21} = 1 - \phi_{ET2}$ into this equation gives $\phi_{ET2} = 1 - [(\phi_{OA} - 1)/(\phi_{ET1} - 1)]$. Thus we estimate $\phi_{ET2} > 75\%$ for *Rb. sphaeroides* and $\phi_{ET2} > 60\%$ for *Rps. acidophila*. The contributions of the Car $S_1 \rightarrow$ BChl EET to ϕ_{OA} are $\phi_{ET1} \times \phi_{21} < 20\%$ for *Rb. sphaeroides* and $\phi_{ET1} \times \phi_{21} < 10\%$ for *Rps. acidophila*. The results of these quantum efficiency calculations are summarized in Table 2.

The Mechanism of Car $S_1 \rightarrow$ BChl Energy Transfer. The mechanism of electronic coupling that promotes Car $S_1 \rightarrow$ BChl EET usually has been discussed in light of the relative merits of Förster versus Dexter energy transfer theories (22, 24, 37). In general, the coupling may be partitioned into a Coulombic contribution V^{Coul}, operative at all separations, and a short-range contribution V^{short} that explicitly depends on interpenetration of the donor and acceptor molecular orbitals. Thus $V = V^{Coul} + V^{short}$. However, V^{short} has been shown previously to be insignificant for interactions between the pigments in LH2 (20, 38).

The transition density cube (TDC) (17) method is very useful for calculating V^{Coul} when the donor and acceptor molecules are closely proximate relative to molecular dimensions, because local interactions between the donor and acceptor transition densities determine the overall coupling. Such details are lost when averaging over wavefunctions to give transition moments. In algebraic form the difference between the dipole approximation and the TDC method is given by

$$|\sum_i q_i \vec{r}_i \| \sum_j q_j \vec{r}_j| / R_{DA}^3 \quad \text{and} \quad \sum_{i,j} q_i q_j / r_{ij} \qquad [1]$$

for discrete charges q_i at position r_i on donor molecule D and charges q_j at position r_j on acceptor A. $r_{ij} = r_i - r_j$, and R_{DA} is the center-to-center separation of D and A.

Zhang *et al.* (19) suggested that the Car $S_1 \rightarrow$ BChl couplings are dominated by Coulombic interactions, V^{Coul}, determined by mixing between the Car S_1 and Car S_2 states. This would result in a Car $S_1 \rightarrow$ BChl transition density with spatial properties resembling the transition density of the Car $S_2 \rightarrow$ BChl transition. If this is the case, scaling down of the Car $S_2 \rightarrow$ BChl electronic couplings, determined previously using the transition density cube method (17), should provide a reasonable estimate of the Car $S_1 \rightarrow$ BChl couplings. The scaling factor is determined by the state mixing between the Car S_1 and Car S_2 states. If Coulombic interactions dominate the Car $S_1 \rightarrow$ BChl couplings, small differences in the positions of the pigments will not affect the couplings as much as for short-range interactions. We therefore assume for the species investigated in this work that the estimated couplings are similar.

In recent work Scholes and Fleming (8) showed that the BChl B800 $\rightarrow$ B850 EET can only be elucidated by introduction of site energy disorder before solving the eigenvalue problem for the B850 acceptor aggregate in each individual LH2, because the assumption of identical B850 eigenstates for each LH2 gives incorrect values for the ensemble average rate, τ_{ET}^{-1}. We

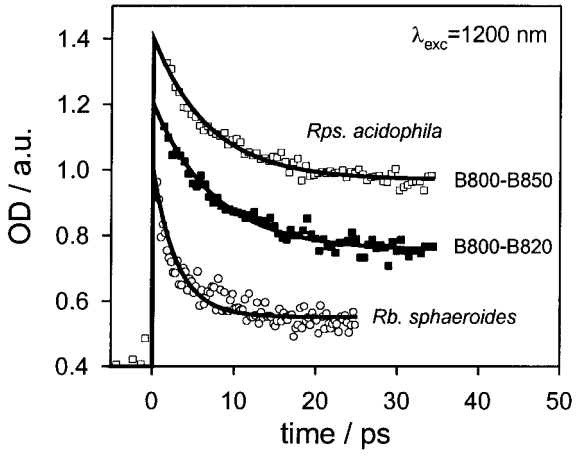

Fig. 4. Time dependence of ESA (λ_{det} = 550 nm) along with monoexponential fits with constant offset of the B800-B850 complex (□, $\tau_{S1} = 7 \pm 0.5$ ps) and the B800-B820 complex (■, $\tau_{S1} = 7.5 \pm 0.5$ ps) of *Rps. acidophila* and LH2 of *Rb. sphaeroides* (○, $\tau_{S1} = 3 \pm 0.5$ ps) observed after TPE (λ_{exc} = 1,200 nm). The traces have been normalized and offset from each other by 0.2.

†Note that this definition of ϕ_{ET1} is different from the definition of ϕ_{ET1} in our former work on LHCII of higher plants and green algae (29). In this work ϕ_{ET1} has to be multiplied with the quantum efficiency for Car $S_2 \rightarrow$ Car S_1 internal conversion after excitation into S_2, ϕ_{21}, to calculate the contribution of Car $S_1 \rightarrow$ BChl EET to ϕ_{OA}, which is the definition of ϕ_{ET1} in ref. 29.

Table 2. Calculated Car $S_1 \rightarrow$ BChl energy transfer time constants and efficiencies

Species	τ_{S1}/ps*	τ_{ET1}/ps	ϕ_{ET1}	$\phi_{OA(9,11)}$	ϕ_{ET2}	$\phi_{ET1}\phi_{21}$	ϕ_{21}
Rb. sphaeroides	1.9 ± 0.5	2.4 ± 0.5	80%	>95%	>75%	<20%	<25%
Rps. acidophila	6.5 ± 0.5	>25	<28%	~70%	>60%	<10%	<40%

$\phi_{OA} = \phi_{ET2} + \phi_{ET1}\phi_{21}$.
*Measured in this work.

anticipate that a quantitative description of the Car $S_1 \rightarrow$ BChl EET will require a similarly detailed theory.

The model we have used for our calculation is described in detail in ref. 8. Briefly, the ensemble average rate of energy transfer is given by

$$\tau_{ET}^{-1} = \frac{2\pi}{\hbar}\left\langle \int_0^\infty \sum_\delta P_\delta |V_{\delta\alpha}|^2 J_{\delta\alpha}(\varepsilon)\mathrm{d}\varepsilon \right\rangle, \qquad [2]$$

where $V_{\delta\alpha}$ is the electronic coupling between the donor state δ and eigenstate α of the acceptor in an individual LH2, calculated by using the electronic couplings in the monomeric site representation, $V_{\mathrm{est.}}^{\mathrm{Coul}}(\mathrm{m})$. P_δ is a normalized population factor, and $J_{\delta\alpha}(\varepsilon)$ is the spectral overlap factor for states δ and α, $J_{\delta\alpha}(\varepsilon) = a_\alpha^{\mathrm{hom}}(\varepsilon) f_\delta^{\mathrm{hom}}(\varepsilon)$. The superscript "hom" specifies that these line shapes are determined only by fluctuations of the bath that have characteristic frequencies faster than that of the EET. Slower fluctuations (e.g., static disorder) are accounted for by the Monte Carlo averaging procedure denoted by the angular brackets in Eq. **2**. The bandwidth of $a_\alpha^{\mathrm{hom}}(\varepsilon)$ and the disorder parameters were derived from three pulse-echo peak shift measurements.

Estimation of the Electronic Couplings Mediating the Car $S_1 \rightarrow$ BChl EET. We modified the B800 $\rightarrow$ B850 EET model by extending the acceptor Hamiltonian by two diagonal elements representing the two B800 BChl in the closest neighborhood to the Car. We used the mirror image of the Car S_1 TPE spectrum of *Rb. sphaeroides* (28) for the donor-fluorescence, $f_\delta^{\mathrm{hom}}(\varepsilon)$. To estimate the electronic couplings in the monomeric site representation, $V_{\mathrm{est.}}^{\mathrm{Coul}}(\mathrm{m})$, we varied the scaling factor for the electronic coupling and the Stokes shift of the mirror image in such a way that the calculation always produced the observed time constant of $\tau_{ET1} \approx 2.4$ ps, *Inset* in Fig. 5*a*. The Car S_1 state 0–0 transition in *Rb. sphaeroides* has been determined to be around 14,000 cm^{-1} (28, 31, 39–41). As can be seen from the inset in Fig. 5*a*, the electronic couplings scaling factor remains very similar (≈0.15) when the 0–0-transition is varied over a wide range. The resulting individual couplings range from 5 cm^{-1} to 26 cm^{-1} (monomeric site representation, see Table 3). The range of these values is in very good agreement with estimates for the necessary couplings from Zhang *et al.* (19) and Damjanovic *et al.* (20). Recently, one of us (C.-P.H.) calculated the Coulombic Car S_1-BChl couplings by using the transition density cube method and time–dependent density functional wavefunctions. The individual couplings obtained in the *ab initio* calculation are in very good agreement with the couplings estimated by the scaling-down procedure (Table 3). Analysis of these results provides strong evidence that scaling down the Car S_2-BChl couplings is appropriate because the Car S_1-BChl Coulomb couplings are dominated by a small mixing of a strongly dipole allowed Car S_2-like configuration as proposed by Zhang *et al.* (19).

In Fig. 5*a* the calculated density of states (DOS) is shown together with the S_1-emission spectrum. Note that the DOS does not necessarily represent the acceptor states in Förster overlap calculations, because each state is coupled differently to the donor states. However, as can be seen in Fig. 5, for *Rb. sphaeroides* there is excellent overlap of donor and acceptor states, which explains the efficient Car $S_1 \rightarrow$ BChl EET observed in this species. Disorder causes the couplings and state orderings in the B850 excitonic states to differ significantly between individual LH2s. Nonetheless, the calculated time constant $\tau_{ET1} \approx 2.4$ ps can be separated into a time constant for Car $S_1 \rightarrow$ B850 EET, $\tau_{B850} \approx 6.7$ ps (15%), and a time constant for Car $S_1 \rightarrow$ B800 EET, $\tau_{B800} \approx 2.8$ ps (85%). The corresponding time constants for *Rps. acidophila* are $\tau_{B850} \approx 11.7$ ps (60%) and $\tau_{B800} \approx 17.5$ ps (40%).

The Car S_1 State in *Rps. acidophila*. We estimate the 0–0 transition energy of the Cars in *Rps. acidophila* by assuming that the S_1 emission spectrum only differs from that in *Rb. sphaeroides* by a shift to lower energies and that the couplings in both species are similar. For *Rps. acidophila* we used the B850 Hamiltonian reported previously, which was obtained by modeling the 77K absorption and CD spectra (8). To determine the 0–0 transition of Car S_1 in *Rps. acidophila,* we shifted the Car S_1 mirror image and calculated the

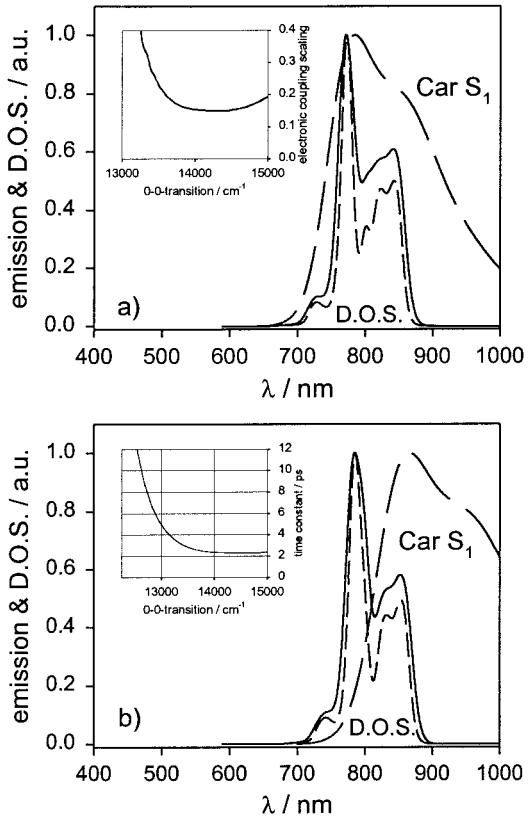

Fig. 5. (*a*) Acceptor DOS in LH2 of *Rb. sphaeroides* calculated with (solid line) and without introducing disorder (short dashed line) before solving the eigenvalue problem for the acceptor aggregate along with Car S_1 emission (long dashed line). Note that the shown DOS is not weighed by electronic coupling. For details see text. (*Inset*) Electronic coupling scaling factor (see text) needed to reproduce the experimentally observed time constant τ_{ET1} as a function of the 0–0 transition of the Car S_1 emission. (*b*) Same results for the B800–B850 complex of *Rps. acidophila*. (*Inset*) Calculated time constants τ_{ET1} as a function of the Car S_1 state 0–0 transition.

Table 3. Car S_1-BChl Q_y couplings in the monomeric site representation estimated by scaling down Car S_2-BChl Q_y couplings, $V^{Coul}_{est.}$, and calculated via *ab initio* methods, V^{Coul}_{TDDFT}

	$B800_A$*	$B800_B$*	$\alpha B850_B$†	$\beta B850_B$†	$\alpha B850_C$†	$\beta B850_C$†
$V^{Coul}_{est.}/cm^{-1}$	26	7	5	7	16	12
V^{Coul}_{TDDFT}/cm^{-1}	31	10	5	9	32	18

*Couplings between Car S_1 and the B800 Chl molecules in the notation of ref. 17.
†Couplings between Car S_1 and the B850 Chl molecules in the notation of ref. 17.

ensemble average time constant by using the same electronic couplings obtained from our *Rb. sphaeroides* calculations. As can be seen from the *Inset* in Fig. 5*b*, time constants larger than the experimentally observed lifetime, $\tau_{10} \approx 7$ ps, are found for 0–0 transitions $\approx<12{,}800\ cm^{-1}$. This value is in very good agreement with S_1 energies of other Cars with 11 conjugated double bonds. However, because the Car S_1 lifetime, τ_{10}, is not known for rhodopin glucoside, this estimate only gives an upper limit, which is valid in the case $\tau_{10} >> \tau_{ET1}$. Of course, differences in the electronic coupling also could contribute to the differences in the EET efficiencies, and in this case the 0–0 transition energy will be underestimated. As in the calculations for *Rb. sphaeroides*, the introduction of disorder did not result in a large difference in the calculated time constant provided we assume that electron–phonon coupling dominates the broadening of the Car S_1 spectrum. However, via some model calculations we found that if the heterogeneous broadening were to contribute significantly to the S_1 spectra, the time constants may change by more than a factor of 2. We also expect that the temperature dependence of the Car $S_1 \rightarrow$ BChl EET can be modeled only by considering Eq. **2**.

Conclusions

By measuring the dynamics of the Car S_1 ESA after TPE, we determined Car $S_1 \rightarrow$ BChl EET time constants in LH2 of the purple bacteria *Rb. sphaeroides* and *Rps. acidophila* without any convolution with dynamics associated with the Car S_2 state or the recently discovered dark state between S_1 and S_2. The energy transfer efficiency was found in *Rps. acidophila* to be $\phi_{ET1} < 28\%$ and in *Rb. sphaeroides* $\phi_{ET1} \approx 80\%$. The Car $S_1 \rightarrow$ BChl EET was modeled by using a detailed theory that suggests that for *Rb. sphaeroides* the time constant for Car $S_1 \rightarrow$ B850 EET is $\tau_{B850} \approx 6.7$ ps (15%) and for Car $S_1 \rightarrow$ B800 EET $\tau_{B800} \approx 2.8$ ps (85%). The corresponding time constants for *Rps. acidophila* are $\tau_{B850} \approx 11.7$ ps (60%) and $\tau_{B800} \approx 17.5$ ps (40%). The individual electronic couplings for the Car $S_1 \rightarrow$ BChl EET are in the order of 5–26 cm^{-1}. A major contribution to the drastic difference in the efficiency ϕ_{ET1} can be explained by a shift of the Car S_1 energy from $\approx 14{,}000\ cm^{-1}$ in *Rb. sphaeroides* to a value of $\approx<12{,}800\ cm^{-1}$ in *Rps. acidophila*.

This work was supported by the Director, Office of Science, of the U.S. Department of Energy under Contract No. DE-AC03–76SF00098. P.J.W. is grateful for financial support from the Deutsche Forschungsgemeinschaft.

1. McDermott, G., Prince, S. M., Freer, A. A., Hawthornthwaitelawless, A. M., Papiz, M. Z., Cogdell, R. J. & Isaacs, N. W. (1995) *Nature (London)* **374,** 517–521.
2. McDermott, G., Prince, S. M., Freer, A. A., Isaacs, N. W., Papiz, M. Z., Hawthornthwaitelawless, A. M. & Cogdell, R. J. (1995) *Protein Eng.* **8,** 43–43.
3. Koepke, J., Hu, X. C., Muenke, C., Schulten, K. & Michel, H. (1996) *Structure (London)* **4,** 581–597.
4. Sundstrom, V., Pullerits, T. & van Grondelle, R. (1999) *J. Phys. Chem. B* **103,** 2327–2346.
5. Nagarajan, V., Johnson, E. T., Williams, J. C. & Parson, W. W. (1999) *J. Phys. Chem. B* **103,** 2297–2309.
6. Zhao, Y., Meier, T., Zhang, W. M., Chernyak, V. & Mukamel, S. (1999) *J. Phys. Chem. B* **103,** 3954–3962.
7. van Oijen, A. M., Ketelaars, M., Kohler, J., Aartsma, T. J. & Schmidt, J. (1999) *Science* **285,** 400–402.
8. Scholes, G. D. & Fleming, G. R. (2000) *J. Phys. Chem. B* **104,** 1854–1868.
9. Angerhofer, A., Cogdell, R. J. & Hipkins, M. F. (1986) *Biochim. Biophys. Acta* **848,** 333–341.
10. Koyama, Y., Kuki, M., Andersson, P. O. & Gillbro, T. (1996) *Photochem. Photobiol.* **63,** 243–256.
11. Frank, H. A. & Cogdell, R. J. (1993) in *Carotenoids in Photosynthesis*, eds. Young, A. & Britton, G. (Chapman & Hall, London), pp. 252–326.
12. Frank, H. A. & Cogdell, R. J. (1996) *Photochem. Photobiol.* **63,** 257–264.
13. Walz, T., Jamieson, S. J., Bowers, C. M., Bullough, P. A. & Hunter, C. N. (1998) *J. Mol. Biol.* **282,** 833–845.
14. Oling, F., Boekema, E. J., Dezarate, I. O., Visschers, R., Vangrondelle, R., Keegstra, W., Brisson, A. & Picorel, R. (1996) *Biochim. Biophys. Acta* **1273,** 44–50.
15. Scholes, G. D., Harcourt, R. D. & Fleming, G. R. (1997) *J. Phys. Chem. B* **101,** 7302–7312.
16. Scholes, G. D., Gould, I. R., Cogdell, R. J. & Fleming, G. R. (1999) *J. Phys. Chem. B* **103,** 2543–2553.
17. Krueger, B. P., Scholes, G. D. & Fleming, G. R. (1998) *J. Phys. Chem. B* **102,** 5378–5386.
18. Sashima, T., Nagae, H., Kuki, M. & Koyama, Y. (1999) *Chem. Phys. Lett.* **299,** 187–194.
19. Zhang, J. P., Fujii, R., Qian, P., Inaba, T., Mizoguchi, T., Koyama, Y., Onaka, K., Watanabe, Y. & Nagae, H. (2000) *J. Phys. Chem. B* **104,** 3683–3691.
20. Damjanovic, A., Ritz, T. & Schulten, K. (1999) *Phys. Rev. E* **59,** 3293–3311.
21. Macpherson, A. N. & Gillbro, T. (1998) *J. Phys. Chem. A* **102,** 5049–5058.
22. Forster, T. (1948) *Ann. Phys.* **2,** 55–75.
23. Forster, T. (1965) in *Modern Quantum Chemistry*, ed. Sinanoglu, O. (Academic, New York), Vol. III, p. 93.
24. Dexter, D. L. (1953) *J. Chem. Phys.* **21,** 836–850.
25. Andersson, P. O., Cogdell, R. J. & Gillbro, T. (1996) *Chem. Phys.* **210,** 195–217.
26. Bautista, J. A., Hiller, R. G., Sharples, F. P., Gosztola, D., Wasielewski, M. & Frank, H. A. (1999) *J. Phys. Chem. A* **103,** 2267–2273.
27. Tavan, P. & Sculten, K. (1987) *Phys. Rev. B* **36,** 4337–4358.
28. Krueger, B. P., Yom, J., Walla, P. J. & Fleming, G. R. (1999) *Chem. Phys. Lett.* **310,** 57–64.
29. Walla, P. J., Yom, J., Krueger, B. P. & Fleming, G. R. (2000) *J. Phys. Chem. B* **104,** 4799–4806.
30. Krueger, B. P., Scholes, G. D., Jimenez, R. & Fleming, G. R. (1998) *J. Phys. Chem. B* **102,** 2284–2292.
31. Chynwat, V. & Frank, H. A. (1995) *Chem. Phys.* **194,** 237–244.
32. Frank, H. A., Bautista, J. A., Josue, J., Pendon, Z., Hiller, R. G., Sharples, F. P., Gosztola, D. & Wasielewski, M. R. (2000) *J. Phys. Chem. B* **104,** 4569–4577.
33. McClain, W. M. (1971) *J. Chem. Phys.* **55,** 2789–2796.
34. Holtom, G. R. & McClain, W. M. (1976) *Chem. Phys. Lett.* **44,** 436–439.
35. Limantara, L., Fujii, R., Zhang, J. P., Kakuno, T., Hara, H., Kawamori, A., Yagura, T., Cogdell, R. J. & Koyama, Y. (1998) *Biochemistry* **37,** 17469–17486.
36. Frank, H. A., Chynwat, V., Desamero, R. Z. B., Farhoosh, R., Erickson, J. & Bautista, J. (1997) *Pure Appl. Chem.* **69,** 2117–2124.
37. Kallmann, H. & London, F. (1929) *Z. Physik. Chem.* **2,** 207–243.
38. Nagae, H., Kakitani, T., Katoh, T. & Mimuro, M. (1993) *J. Chem. Phys.* **98,** 8012–8023.
39. Frank, H. A., Desamero, R. Z. B., Chynwat, V., Gebhard, R., van der Hoef, I., Jansen, F. J., Lugtenburg, J., Gosztola, D. & Wasielewski, M. R. (1997) *J. Phys. Chem. A* **101,** 149–157.
40. Shashima, T., Shiba, M., Hashimoto, H., Nagae, H. & Koyama, Y. (1998) *Chem. Phys. Lett.* **290,** 36–42.
41. Fujii, R., Onaka, K., Kuki, M., Koyama, Y. & Watanabe, Y. (1998) *Chem. Phys. Lett.* **288,** 847–853.